Optical phase-locked loop phase noise in 5G mm-wave OFDM ARoF systems

Optics Communications 526 (2023) 128872

Contents lists available at ScienceDirect

Optics Communications

journal homepage: www.elsevier.com/locate/optcom

Optical phase-locked loop phase noise in 5G mm-wave OFDM ARoF systems

Delphin Dodane [a], Javier Pérez Santacruz [b,*], Jerome Bourderionnet [a], Simon Rommel [b], Gilles Feugnet [a], Antonio Jurado-Navas [c], Laurent Vivien [d], Idelfonso Tafur Monroy [b]

[a] Thales Research & Technology, 1 avenue Augustin Fresnel, 91767 Palaiseau Cedex, France
[b] Institute for Photonic Integration, Eindhoven University of Technology, 5600MB Eindhoven, The Netherlands
[c] Wireless Optical Communications Lab., University Institute of Telecommunication Research (TELMA), University of Málaga, CEI Andalucía Tech., Málaga E-29071, Spain
[d] Université Paris-Saclay, CNRS, Centre de Nanosciences et de Nanotechnologies, 10 boulevard Thomas Gobert, 91120 Palaiseau, France

ARTICLE INFO

Keywords:
5G
Phase noise
OPLL
ARoF
OFDM
Mm-wave

ABSTRACT

The use of millimeter-wave (mm-wave) frequencies is required in order to support the increasing number of connected devices expected from the fifth generation (5G) of mobile communications. Subsequently, the generation of radio-frequency (RF) carriers ranging from 10 GHz to 300 GHz and their transport through optical distribution network (ODN) is a key element of the future 5G fronthaul. Optically assisted RF carrier generation is one of the most promising solutions to tackle this issue, allowing a wide use of analog radio-over-fiber (ARoF) architectures. However the main limitation of these optical methods is related to the finite coherence of lasers sources, which can dramatically degrade data transmission in analog formats. To mitigate its impact, the use of orthogonal frequency-division multiplexing (OFDM) as the 5G standard allows employing efficient phase noise compensation algorithms. Therefore, in this study, we present an experimental demonstration of a mm-wave generation technique based on an optical phase-locked loop (OPLL) that fulfills the frequency specifications for 5G. Then, an algorithm is introduced that improves data recovery at reception and reduces the impact of a possible high phase noise carrier. Finally, a back-to-back data transmission experiment is performed, demonstrating the efficiency of the algorithm to reach the 5G requirements. These results emphasize the use of OPLLs as a viable solution to generate mm-wave carriers for 5G and beyond.

1. Introduction

The fifth generation (5G) of mobile communications has been thought to support one of the widest increase in data rate in telecom history [1], namely the incoming internet of things (IoT) and its underlying galaxy of connected devices. These non-human users, or let say machines, are expected to constitute the major part of the data exchanges within the 2020 decade [2], and the current network architecture is not capable to satisfy such a high demand. One of the reasons is that usual frequency bands are already fully occupied in many countries and the natural solution to solve this is to look toward the next available bands: mm-wave frequencies (<300 GHz) [3,4]. The benefits are obvious since there is tens of times more available spectrum than in the traditional sub-6 GHz frequency range. However, the shorter range of mm-wave, despite allowing massive paralleling and optimized spatial efficiency [5,6], sets always more stringent constraints in terms of consumption, compactness and costs [7]. This statement emphasizes the limits of the current widespread digital radio-over-fiber (DRoF) architecture and especially its lack of scalability toward the increasing number of cells [8]. Therefore the hardware implementation of the fronthaul network has to be re-thought, leading to a progressive shift from digital to analog radio-over-fiber (ARoF) [9–11].

The utilization of ARoF supports the need for highly scalable low-complexity mm-wave cells, which number will rise substantially due to their short range (<200 m), resulting in network densification. While allowing few technologies to be more efficient, as for instance spatial division multiplexing (SDM) and phase array antennas (PAA), ARoF is able to handle with both the need for simple and compact remote units (RU) and a more complex analog processing [12]. It relies on the centralization of all the processing in the central office (CO), including digital-to-analog (DAC) conversion, in order to feed mm-waves cells with a “ready-to-emit” signal. The cornerstone of this architecture is actually to replace a mm-wave RF source at the RU by a remote-fed *optical* local oscillator (LO) that can be sent through the optical distribution network (ODN) together with the processed data.

Yet, mm-wave optical LO generation is challenging because the RF emitted signal results from the beating of two optical tones, which usually results in a rather low purity RF carrier compared to electronic sources. A diversity of methods already exist to deal with optically

* Corresponding author.
E-mail address: j.perez.santacruz@tue.nl (J.P. Santacruz).

https://doi.org/10.1016/j.optcom.2022.128872
Received 14 March 2022; Received in revised form 18 July 2022; Accepted 9 August 2022
Available online 13 August 2022

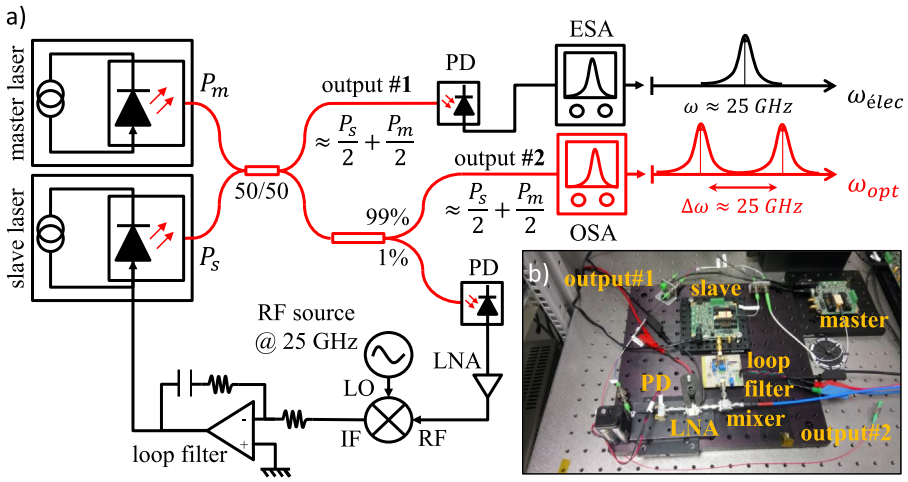

Fig. 1. (a) Description of the OPLL setup and b) picture of the experiment. Optical parts of the setup are depicted in red and electrical ones in black. PD: photodiode, LNA: low-noise amplifier, OSA/ESA: optical/electrical spectrum analyzer.

assisted mm-wave generation, among which self-heterodyne solutions are very common, as for instance suppressed-carrier Mach–Zehnder modulators (SC-MZMs) [13,14], mode-lock lasers (MLLs) or various other frequency combs [15]. As these methods generate intrinsically multiple optical carriers they require also amplifiers as well as filters to get rid of unwanted harmonics. On the other hand, purely heterodyne methods utilize optical tones from different lasers, generally implying to tackle with phase noise issues [16,17]. However, recent progress in the field of integrated semiconductor lasers (SCLs) shows very promising results, allowing fabricating compact high-power low-linewidth sources [18,19]. Another well-known heterodyne approach is to make two sources artificially coherent through the use of an optical phase lock loop (OPLL) [20–25]. This method is derived from SCL frequency stabilization mechanisms and benefits from a high available optical power, even though it is very dependent from feedback electronics and exhibits generally higher phase noise than self-heterodyne techniques.

Moreover, the 5G adopted standard being OFDM, phase noise of the mm-wave carrier becomes an even more stringent requirement to maintain orthogonality between subcarriers [26,27]. To solve this, two approaches are to be considered : the development of lower phase noise sources and the improvement of transmission robustness by the mean of compensation methods. In the latter, OFDM properties are combined with numerical algorithms to recover data even with high carrier phase noise. By mitigating the impact of optical coherence these algorithms are a path to relax the constraints on sources purity [28], allowing a widespread use of cheap and common laser sources in OFDM mm-wave transmissions. In particular this can be used to make OPLLs a better candidate for the generation of remote-fed optical LOs and it represents a very promising and viable method for the new 5G ARoF fronthaul.

In this manuscript we first present in Section 2 an OPLL implementation that allows generating two high-power locked optical tones for mm-wave carriers with offset frequencies up to 25 GHz (K-band) based on commercially available solutions. We also discuss the interest of using an OPLL compared to other methods, based on their respective phase noise performances. Section 3 will be dedicated to the description of a new phase noise compensation algorithm aimed to reduce the impact of phase noise over OFDM and complex data formats. Moreover, the proposed algorithm will be compared with a more traditional method for compensating the phase noise. Then, in Section 4, we apply algorithms depicted in Section 3 to the OPLL of Section 2 in order to evaluate how much of the intrinsic OPLL phase noise can be mitigated in the scope of a mm-wave transmission in the K-band. Finally, Section 5 will provide some remarks as well as perspectives toward future work.

2. Optical phase lock loop

The OPLL implemented in this work has been previously used in another transmission experiment [8], including multi-core fiber and free space transmission with real-time processing. However, results have shown that it was not suitable in that case, the OPLL phase noise being still too high for real-time processing. The main goal of this work is then to demonstrate that a dedicated digital signal processing (DSP) can circumvent this issue and make the OPLL suitable for 5G fronthaul. In this section, we will first describe the experimental implementation of our OPLL based on commercially available bulk components and working in the K-band carrier frequencies. Then, an evaluation of the phase noise performance of the loop is carried out to quantify accurately the amount of noise that has to be overcome by the mitigation algorithms. It is also compared with phase noise in several mm-wave optically assisted generation methods and a discussion on the interest of using an OPLL for OFDM transmission in ARoF is carried out.

2.1. OPLL setup

In its electrical version, the phase lock loop (PLL) [29] has become a widespread technique to deal with clock signals synchronization, frequency up-conversion and demodulation. The OPLL is no more than its optical equivalent and is aimed to compensate the phase noise difference between two laser sources. The resulting beating of both sources is then apparently “free” from phase noise since the sources are made artificially coherent within the operating bandwidth (BW) of the loop.

The overall setup is described in Fig. 1 and is aimed to up-convert an OFDM signal from baseband (BB) to mm-wave n258 band, centered at 25 GHz. It is built using two commercial 1.55 µm distributed feedback (DFB) lasers manufactured by Gooch & Housego (100 kHz linewidth, up to 100 mW optical power). These DFB lasers are butterfly-packaged and driven using low-noise current sources commercially available from Koheron. The main assets of the current drivers are their relatively small footprint (7.5 × 8.5 cm^2), which limits the loop propagation delay, and their modulation entry allowing a dynamic frequency tuning up to 10 MHz. DFB lasers are thermally tuned so that their frequency offset matches the desired mm-wave carrier frequency and then optical signals are mixed using fiber couplers. In order to minimize propagation delay within the feedback loop, these couplers have been shortened down to ≈20 cm each (including coupler itself, fibers and pigtails). A 2 × 2 coupler operates the mixing and ensures both tones are in quadrature while a 99/1 coupler is used to extract a small portion of the optical power to operate the feedback. This setup provides two

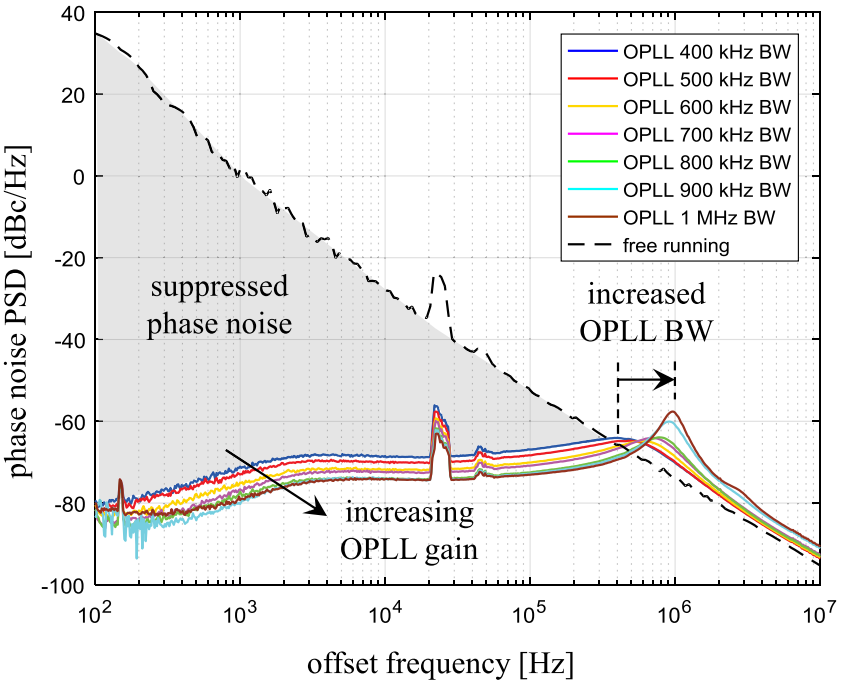

Fig. 2. Experimental measurements of the single sideband (SSB) OPLL phase noise for different open loop gains/BW. Beating is centered on 25 GHz. Gray area represents the suppressed phase noise compared to free running operation.

equivalent outputs that can be used independently. In Section 4 for instance one will feed the transmission experiment while the other will monitor the locking. The 1% output serves as error signal and is sent on a high-speed photodiode (PD), followed by a low-noise amplifier (LNA) and a wide-band mixer which role is to down-convert the error signal to baseband. Finally, the error signal is fed trough a single-amp proportional integral (PI) corrector and applied to the modulation entry of the laser driver. At maximum power working point OPLL outputs deliver 100 mW each, which means a total of 23 dBm available optical power. Such an implementation consists in delivering a locked two-tones high-power optical signal which can be utilized in many ways: it can be sent to remote unit to serve as an RF LO [8,11], it can also be directly modulated with data or for instance be filtered in order to process one of the tone while keeping the coherence with the second tone for a final beating. Finally, it can be combined with complex photonic integrated circuits (PICs), as for instance an optical beamforming network [30], in the context of future 5G and beyond fronthaul. The main asset is to have a powerful coherent input that can be split into several paths without using fibered amplifiers nor on-chip semiconductor amplifiers.

2.2. OPLL performance

As the OPLL described in the previous section is based on DFB lasers then it is necessary to operate the feedback on the laser gain section. Yet, it is well-known that this intrinsically limits the OPLL BW [31]. Indeed, a competition between thermal and carrier tuning of the laser frequency takes place in the DFB laser and the switch between them occurs in the MHz range, reversing the sign of the feedback [32,33]. This cannot be easily nor efficiently overcome and that is why it represents an intrinsic limit of the loop. However, the loop performance can be dramatically lowered by another factor, namely the loop delay, which can be even more limiting than the laser frequency tuning. Here, as mentioned earlier, great care has been taken to shorten the optical path within the feedback loop. This results in a loop delay of the order of 25 ns, that is low enough to make the laser becoming the limiting factor. Then, in the following, the maximum OPLL BW achieved with this implementation is no more than 1 MHz, which is lower than what can be done for instance with sampled-grating distributed Bragg reflector (SG-DBR) lasers [34,35].

The operating range of the OPLL is dependent from each component BW and in particular PD, LNA and mixer. In the current implementation the locking has been demonstrated from 17 GHz to 26 GHz, which are the lower BW of the LNA and the upper BW of the PD, respectively.

Finally, the OPLL implemented here is perfectly stable over long times which makes it proper to transmission experiments and phase noise measurements, especially in the region close to carrier frequency (here down to 100 Hz). Such a measurement is done using an electrical signal source analyzer (Keysight E5052B, equipped with its 26 GHz down-converter) fed with one of the OPLL outputs through a high-speed PD. We present in Fig. 2 measurements of the locked OPLL phase noise for various loop gains, leading to a set of OPLL BW ranging from 400 kHz to 1 MHz. The optical phase noise of the free running beating tone of the lasers is also shown (dot curve) and thus one can observe that the OPLL suppresses a high amount a phase noise (gray area) compared to the free-running operation. The peak in the phase noise located around 20 kHz offset frequency is an electronic noise coming from the driving circuitry. The equation giving the locked phase noise of the beating shown in Fig. 2 is the following [36]:

$$S_{\varphi}^{OPLL}(\nu) = (S_{\varphi_m}(\nu) + S_{\varphi_s}(\nu)) \cdot |1 - H(2i\pi\nu)|^2 + S_{\varphi_{RF}}(\nu) \cdot |H(2i\pi\nu)|^2 \quad (1)$$

with indexes m and s referring to master and slave respectively, H being the closed loop transfer function and $S_{\varphi_{RF}}$ the phase noise of the RF source. The effect of an increasing open loop gain (equivalent to $H \rightarrow 1$) on the phase noise of the beating is clearly shown in Eq. (1) and Fig. 2: the higher the gain the lower the optical phase noise of the beating, especially at low offset frequencies. The counterpart is that the OPLL is pushed toward its stability limit, resulting in the appearance of a peak in the phase noise. This defines the actual BW of the loop, i.e. the offset frequency at which the open loop transfer function becomes lower than unity. Above this particular frequency the beating tone phase noise progressively tends toward the free-running phase noise. That peak appears to be problematic because its contribution to the total phase error variance of the beating is high. Indeed, the single

Table 1
Phase error variance values for various OPLL BW. Integration is made from 100 Hz to 10 MHz.

OPLL BW [kHz]	400	600	700	900	1000
σ_φ^2 [rad^2]	0.3266	0.2949	0.3395	0.5885	0.8025

sideband (SSB) phase error variance is related to the phase noise power spectral density (PSD) by the following relation [37]:

$$\sigma_\varphi^2 = \int_0^\infty S_\varphi(\nu) d\nu \tag{2}$$

Since optical phase noise tends toward zero at high frequencies from the carrier, then Eq. (2) implies that phase error variance tends asymptotically toward a finite value, which is mostly imposed by the peak located around the loop BW in our case (see Fig. 2 brown curve around 1 MHz). Some phase error variance values for different OPLL BW are given in Table 1 (integrated from 100 Hz to 10 MHz), from which we can see that σ_φ^2 is more than doubled when in stability limit compared to great stability/low BW. Yet it has to be compared to the free running phase error variance which is 1.77×10^5 rad^2 (from the dot curve of Fig. 2), proving that the OPLL method can considerably reduce the phase noise of an heterodyne beating even for high phase noise lasers.

2.3. Performance comparison with other optical two-tone generation techniques

To give an interpretation of our OPLL performances described in the previous subsection we have to remind that our aim is to mitigate an heterodyne optical beating tone phase noise using specific algorithms. This approach can also be applied to a completely free running lasers beating. In our case, and presumably using any semiconductor lasers with higher linewidths, this will lead to a beating phase noise much too high to be mitigated by our algorithms.

One of the reasons is linked to the low offset frequency part of the phase noise (< 1 kHz), which actually describes the slow frequency drift of the beating tone and has to be kept low to satisfy the 5G standard [38]. For the sake of comparison, we measured the free beating tone of very pure fiber lasers (NKT photonics E15, < 10 Hz linewidth) over the same offset frequency range (100 Hz to 10 MHz) and found 14 rad^2, namely one to two orders of magnitude higher than levels showed in Table 1. The main contribution to this value is located at few hundreds Hz offset frequency and below. The advantage of the OPLL regarding this point is that it cancels the lower part of the free running phase noise, getting rid of the slow frequency drifts. Ultimately, the OPLL phase noise is limited by the purity of the RF source used to down-convert the error signal within the loop (Eq. (1)). This basically means that slow variations of the locked optical beating reproduce those of the RF source, which is extremely stable over time. A comparison of performances, advantages and drawbacks of some mm-wave generation methods are listed in Table 2.

The other main reason is more obvious and is linked to phase noise for offset frequencies above 1 kHz: these variations are fast enough to make the phase fluctuate within the duration of one OFDM symbol, which can severely impact the transmission. That is why the phase error variance, and consequently the phase noise of the laser sources, is critical for data transmission with analog modulation formats like QAM because the information is partially encoded into the phase of the transmitted signal. As a consequence a high carrier phase noise can lead to wrong interpretation of a transmitted bit, with high order modulation being even more sensitive. In addition to this, the OFDM method relies on the orthogonality between subcarriers which condition is also dependent on phase noise in order to be kept valid. Usually it is considered that a 10° standard deviation (0.03 rad^2) over a frequency range from 1 kHz to 1 GHz is a reasonable target [24], which is one order of magnitude below the best performance of our implementation. To face this, self-heterodyne methods like external modulation by using MZMs are interesting because they will reproduce not only slow phase variations but the whole phase noise spectrum of the RF source. This will lead to an overall much better phase noise performance though it is still limited in terms of architecture complexity. For instance it is heavily dependent on optical filtering and amplifiers, as well as equalizing optical paths to keep optical coherence. These aspects are also included in Table 2.

Table 2
Comparison between various approaches for generating optical two-tone signals.

Criteria	Free-running lasers	OPLL	Ext. modulation
Phase error variance[a] in rad^2	> 14[b]	≈ 0.5	typ. 10^{-4} to 10^{-5}[c]
Power efficiency	Very high	High	Low
Frequency range	< 100's THz	10's GHz	10's GHz
Architecture complexity	Low	Medium	High

[a]From 100 Hz to 10 MHz.
[b]With commercially available sources.
[c]For a commercial RF source in the mm-wave.

Taking into account all points listed in the Table 2 we considered that using a self-heterodyne method, even though it gives better phase noise, requires too many elements and is a less flexible approach for 5G fronthaul. On the contrary, free beating is the simplest solution but still suffers from phase noise issues at frequencies close to the carrier, even for low linewidth lasers. Our approach, using an OPLL, is to benefit from both methods to get a highly stable beating combined with great flexibility and high available power. The choice of DFB laser diodes is driven by the will to use commercial low cost and small footprint components at the expense of the phase noise, which has then to be mitigated to lower its impact on the OFDM transmitted signal. This will be done using compensation algorithms, which are described in the next section.

3. Phase noise compensation methods

Phase noise compensation has already been performed in optical coherent systems [39,40]. Nonetheless, in the research literature of optical communications, single-carrier (SC) modulation formats are mainly utilized. The signal degradation induced by the phase noise in SC modulation formats is less than in multi-carrier (MC) signals such as OFDM. This is because the symbol duration of SC modulation formats is typically shorter than in the OFDM scenario. Moreover, OFDM signals suffer from severe impairments due to phase noise. As high phase noise levels are associated with optically assisted mm-wave generation, it is then one of the major performance limiting factors for using this method within OFDM systems. Thus compensation techniques are more complex in mm-wave OFDM scenarios. The works of [41–43] are examples of OFDM transmission over a mm-wave ARoF setup. However, in these works, the employed subcarrier spacing of the transmitted OFDM signal is larger than in the 5G numerology, lowering phase noise impact. The investigation carried out in [44] aims to bring experimental assessments on the transmission of OFDM signals with 5G numerology over a mm-wave ARoF setup under different phase noise levels. To go further, the work we present here is, to the best of the authors' knowledge, the first experimental demonstration of OFDM signal transmission with 5G numerologies over a mm-wave ARoF setup based on OPLL two-tone generation. Since phase noise is the main impairment due to the use of 5G numerologies and OPLL configuration, the utilization of DSP algorithms to compensate for the phase noise is essential for proper communication performance.

This section explains the fundamentals of the used methods to compensate the phase noise produced by the aforementioned OPLL implementation. In particular, two digital signal processing methods are utilized: RF-pilot assisted method and a novel algorithm named hybrid scattered pilots with decision feedback (SPDF). In this section,

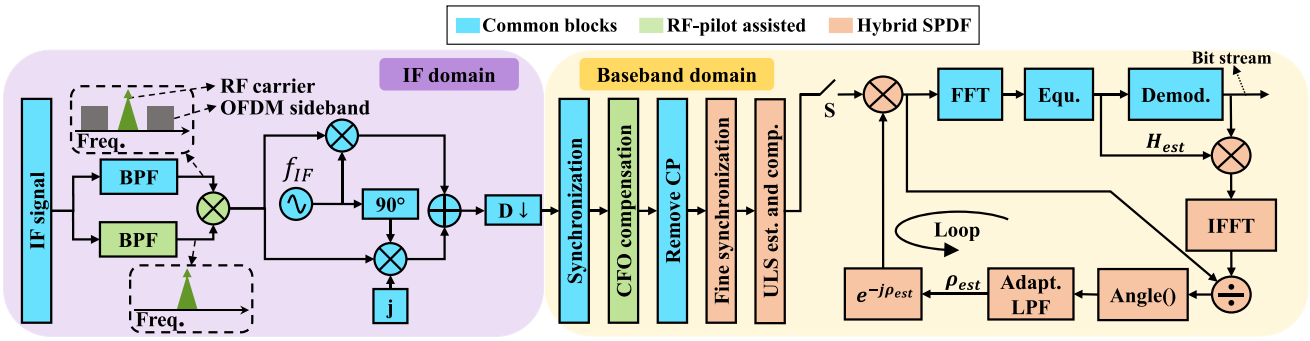

Fig. 3. DSP block diagram in the receiver side for both employed algorithms to compensate the phase noise: RF-pilot assisted (green) and hybrid SPDF methods (orange). Blocks depicted in green and orange are exclusive to the related employed method while blue blocks are common for both.

we describe these two methods, while in next section we will compare their performances using the OPLL transmission setup.

The RF-pilot assisted method relies on using the carrier associated with the modulated signal to compensate for the phase noise at the receiver side. It can be applied to any modulation format and is also used for instance in [45]. However, the RF-pilot assisted method introduces an additional process in the intermediate frequency (IF) domain, increasing the complexity of the system because a higher number of samples are processed in this domain, with respect to BB domain. Furthermore, the RF-pilot assisted method requires to transmit the RF tone through the transmission channel, reducing the available bandwidth, which is already highly limited in wireless scenarios. Moreover, transmitting the RF tone reference throughout the communication system increases the overall power of the transmitted signal, which reduces the power level of the data signal at the output of devices such as RF amplifiers and RF mixers. For proper extraction of the phase noise by using the RF-pilot assisted method, the signal-to-noise ratio (SNR) level of the received RF reference carrier must be sufficiently high. Therefore, there is a trade-off between SNR of the received data signal and phase noise compensation efficiency of the RF-pilot assisted method.

For a mm-wave mobile scenario, the RF reference carrier is needed to be sent through wireless channel if applying the RF-pilot assisted method. This fact implies a reduction of the spectrum efficiency, which is quite important in wireless communications. Another drawback of the RF-pilot assisted method is that it operates in the IF domain, increasing the sampling rate requirements in the case of a DSP implementations. Besides, low received power is one of the major limitations in mm-wave wireless. Thereby, all the mentioned drawbacks related to the RF-pilot assisted method make baseband DSP algorithms for phase noise compensation a more suitable option for mm-wave wireless systems, as it does not require any RF tone reference.

As a parallel solution, we present a hybrid SPDF algorithm that operates only at baseband and do not require an RF reference carrier, being more well-suited for mm-wave wireless communications than the aforementioned RF-pilot assisted method. Furthermore, DSP in the IF domain is not needed and analog-to-digital converters (ADC) with lower sampling frequency can be used. However, this hybrid SPDF can only be applied to OFDM signals, combining two strategies to estimate the phase noise [46]: a coarse initial phase noise estimation is performed using the scattered pilots of the OFDM signal and, then, a fine phase noise estimation is achieved by applying decision feedback in the received OFDM signal. By targeting a determined error vector magnitude (EVM) output value, this decision feedback method is more flexible in terms of complexity to mitigate the phase noise than the scattered pilots method because it can be iteratively performed in a loop [44,46]. Therefore, once the EVM target value is reached, the loop procedure can be finalized. The employed strategy of the decision feedback methods is based on recovering the time-domain transmitted signal to estimate the phase noise. Nevertheless, iterative decision feedback methods often suffer from convergence issues because its performance is intrinsically related to the initial bit error rate (BER) of the received signal. In the other hand, scattered pilots algorithms are more robust since they do not depend on the received BER. Therefore, a scattered pilots method can be performed before a decision feedback method to combine the benefits of both strategies: robustness, accuracy, and flexibility in the phase noise estimation. These are the reasons why hybrid SPDF is proposed as a suitable solution to compensate the inherent high phase noise of mm-wave OPLL systems for an OFDM communication.

In our implementation, the unconstrained least-squares (ULS) approach is the chosen scattered pilot method to obtain an initial phase noise estimation by using the discrete cosine transform (DCT) [47]. Yet, there exists other scattered pilot algorithms that could have also been implemented in our hybrid SPDF [46]. Concerning the decision feedback method, some previous work on the topic [44] will be adapted and can prove to be very effective here because it synergizes well with the OPLL dynamic behavior by the mean of an adaptive low-pass filter (LPF).

Fig. 3 shows the DSP receiver block diagram employed to perform the aforementioned algorithms. This receiver process assumes an OFDM signal with an IF at the reception. In Fig. 3, the cyan blocks correspond to the common blocks for both algorithms. The green and orange blocks refer to the particular processing for the RF-pilot assisted and the hybrid SPDF methods, respectively. First, in the IF domain, the IF signal is filtered by a band-pass filter (BPF), keeping the RF carrier and one of the OFDM sidebands. If RF-pilot is applied then the IF signal is split into a secondary branch, where the sole RF-tone is obtained by filtering the rest of the frequency components with a second BPF [45]. Then, the isolated RF-tone can be multiplied by the IF signal of the other branch, compensating the phase noise contained in this RF-tone. Next, an IF demodulation and down-sampling processes are performed to convert the IF signal into the baseband domain. The IF domain exposed in Fig. 3 can be done by hardware, reducing the requirements for the DACs. However, a specific narrowband BPF must be designed in the RF-pilot assisted case.

Now in the baseband domain of Fig. 3, a synchronization process is performed by employing the preamble of the transmitted signal. Then, a coarse frequency offset (CFO) compensation is used when applying the RF-pilot assisted method because this method only reduces the signal deterioration due to the phase noise [45]. On the other hand, the hybrid SPDF method can avoid the CFO compensation because this method compensates both phase noise and frequency offset (FO). Next, the cyclic prefix (CP) of the OFDM signal is removed. Finally, for the RF-pilot assisted method, the classical OFDM receiver is performed, namely fast Fourier transform (FFT), frequency-domain channel equalization, and final demodulation. The zero-forcing technique is the selected channel estimation method due to its simplicity. For the hybrid SPDF, an initial phase noise estimation is achieved using the ULS algorithm. However, a fine synchronization must be performed before

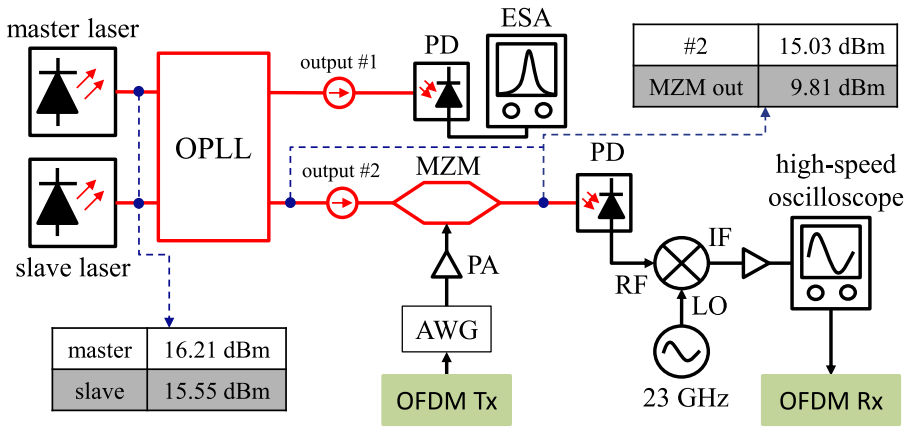

Fig. 4. Description of the OFDM setup. The OPLL output is intensity modulated using an arbitrary waveform generator fed with the OFDM Tx signal. An oscilloscope is used to make the acquisition of the Rx down-converted signal.

this initial estimate because the ULS algorithm is highly sensitive to synchronization errors. This fine synchronization process is realized by calculating the time position of the first ray in the estimated impulse channel response. After the ULS process, the decision feedback loop is realized for the hybrid SPDF method. The procedure of this loop aims to estimate and compensate the residual phase noise that was not compensated in the ULS block. The strategy to compensate for the phase noise in the decision feedback loop consists of estimating the transmitted OFDM signal. With the estimate of the OFDM transmitted signal, the phase noise can be estimated later by performing an inverse process than that of the communication channel [44]. Hence, the phase noise estimate is improved by using an LPF whose spectrum shape is linked to the phase noise PSD [44]. The filtered phase noise estimate is then used to compensate the received OFDM signal. As a consequence, when performing another iteration in this loop, the number of errors after the demodulation block is lower than in the initial iteration and a better phase noise estimate can be obtained. Thereby, this decision feedback loop can be iterated to improve the final yields. Furthermore, better performance can be achieved if spectrum shape of the inner LPF of the loop is modified according to the number of iterations.

4. Experimental study of OPLL phase noise impact on OFDM mm-wave transmitted signal

In this section, we will first describe how the OPLL from Section 2 is implemented into an OFDM back-to-back experiment. Then, the obtained results are analyzed through the use of the phase noise compensation method described in Section 3 to study the intrinsic tolerance of OFDM to the OPLL phase noise.

4.1. Experimental setup

The experimental setup is described in Fig. 4 and is constituted as follows: one of the OPLL outputs is used to monitor the locking through the use of a PD, and the other output is fed through a Mach–Zehnder modulator to encode the OFDM data. The data are generated by the mean of an arbitrary waveform generator (AWG) (Tektronix 25 GSa/s) and its spectral band is centered on 1 GHz IF frequency. A power amplifier (PA) is used to drive the modulator, which is biased at its quadrature point. Then, the modulated signal is directly detected with a high-speed PD and down-converted with a mixer to ≈2 GHz in order to avoid spectral aliasing. The obtained temporal trace is then post-processed with the phase noise compensation algorithm described in Section 3.

The signal analyzed here is the one which would be transmitted to a RU for free space emission in a real fronthaul scheme. Potential phase fluctuations due to fiber dispersion and free space propagation are not accounted here as our goal is to study the OPLL contribution to phase noise of the RF carrier. Yet, the aforementioned contributions are typically small compared to OPLL phase noise in our case. In order not to saturate the PD used to convert the K-band Tx signal, the OPLL setting point is fixed approximately at half the maximum power of the lasers. While the phase noise of the lasers is slightly lower in this case, most of the difference is due to thermal effects happening at high currents. These effects are located at frequencies close to the carrier and are perfectly corrected by the loop so that the OPLL phase noise is the same whether it is used at half or maximum optical power. Optical powers measured at the different stages of the setup are shown in Fig. 4.

Table 3
OFDM configuration parameters.

Config.	1	2	3	4	5
Δf [KHz]	15	30	60	120	240
N	2^{14}	2^{13}	2^{12}	2^{11}	2^{10}
T_{cp} [μs]	4.8	2.4	1.2	0.6	0.3

The different phase noise configurations that will be investigated here corresponds to BW of 400 kHz, 700 kHz and 1 MHz, with a maximum factor of 2.5 in their phase error variances. Modulation formats used in the experiment are 16-QAM and 64-QAM, for all 5G subcarrier spacings (15, 30, 60, 120 and 240 kHz) [38]. The main parameters of the different employed OFDM numerologies are shown in Table 3: subcarrier spacing (Δf), total number of subcarrier (N), and CP period (T_{cp}). For all the OFDM configurations, the total BW is 245.76 MHz, the percentage of active subcarriers is 80.5 %, and one pilot subcarrier is inserted on every 12th active subcarrier.

4.2. Experimental results

For each of the tested configurations described above we performed a set of different measurements in order to have significant statistical evaluation. Figs. 5 and 6 show the experimental results for both receiver algorithms applied to the OPLL transmitted OFDM signal: Fig. 5 corresponds to the RF-pilot assisted method while Fig. 6 refers to our hybrid SPDF method.

The experimental results using the RF-pilot assisted method are presented in terms of EVM in percentage as a function of subcarrier spacing, for different bandwidths of the OPLL loop filter (see Fig. 5). Moreover, 16-quadrature amplitude modulation (QAM) and 64-QAM constellations are also presented in Fig. 5(a) and (b), respectively. From Fig. 5, it can be noticed that the EVM decreases as the subcarrier spacing value increases. This is explained by the fact that lower subcarrier spacing is more prone to interference [44]. It can also be noticed that there is a slight increment of the EVM for 240 kHz of subcarrier spacing. The reason of this EVM behavior is due to the large frequency

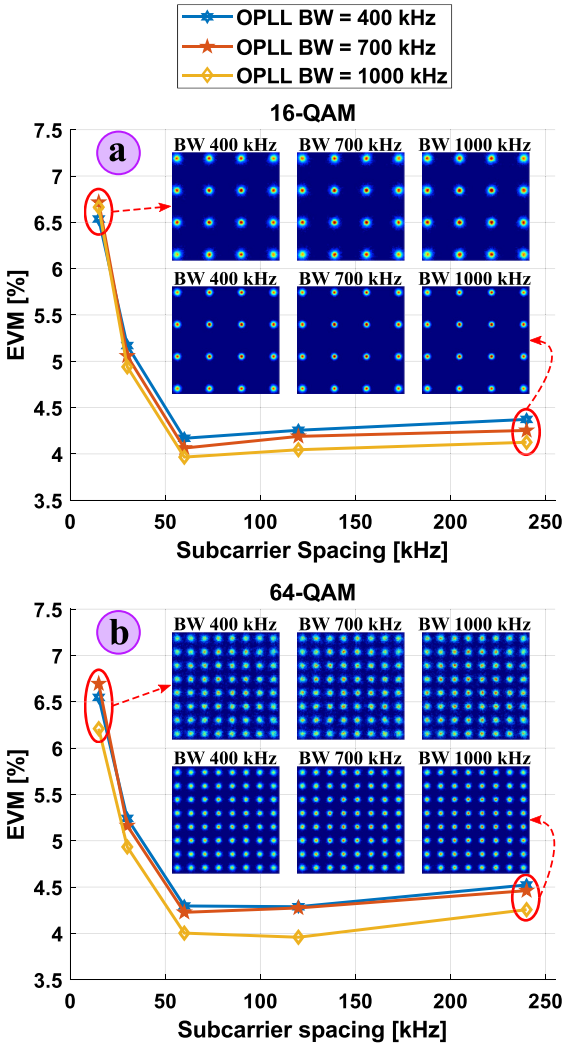

Fig. 5. Experimental results employing the RF-pilot assisted method of Section 3. The results are presented in terms of EVM as a function of the subcarrier spacing for different modulation orders (16-QAM and 64-QAM). These results are also compared concerning the bandwidth of the loop filter in the OPLL block.

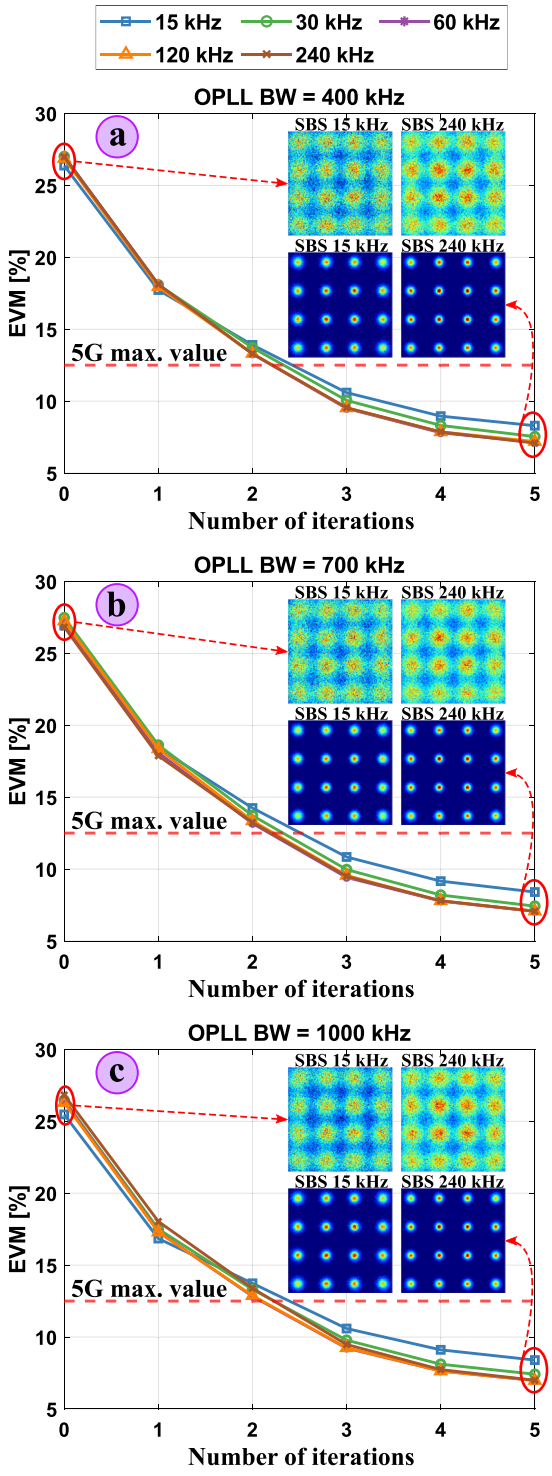

Fig. 6. Experimental results utilizing the hybrid SPDF method of Section 3. The EVM curves are exhibited as a function of the number of iterations of the decision feedback loop for 16-QAM modulation.

spacing between pilots and the lower total number of pilots for higher subcarrier spacing values, leading to a poorer channel estimation. Furthermore, in Fig. 5, the distribution of the constellation points are depicted for the different OPLL configurations and for subcarrier spacing values of 15 kHz and 240 kHz. The experimental EVM results by applying the RF-pilot assisted method are under the EVM 5G threshold for both used modulation orders (12.5% for 16-QAM, and 8% for 64-QAM [38]). In addition, one can notice that EVM is slightly better for 1 MHz OPLL BW, although its phase error variance is higher. This behavior could be due to the lower carrier phase noise within the BPF BW used to isolate the RF tone.

The graphs of Fig. 6 are the experimental results obtained by employing the proposed hybrid SPDF method with 16-QAM modulation format. These results are presented in terms of EVM as a function of the number of iterations in the decision feedback loop for different BWs of the OPLL and for the different 5G numerologies. In Fig. 6, the iteration zero refers to the EVM in the output of the channel equalizer without any iteration in the decision feedback loop of Fig. 3. Examining Fig. 6, it can be noticed that the EVM decreases with the number of iterations of the decision feedback loop. Therefore, for 16-QAM the decision feedback adequately converges for all the different 5G numerologies and OPLL configurations. On the other hand, the 64-QAM has not been successfully treated with our hybrid SPDF algorithm. This is essentially due to the fact that 64-QAM is more sensitive to phase fluctuations than 16-QAM and the initial constellation, before the first iteration, is too noisy to allow the algorithm to converge. At this stage, the algorithm is still very dependent from the initial EVM to work properly and our OPLL phase noise is not low enough to consistently deal with 64-QAM.

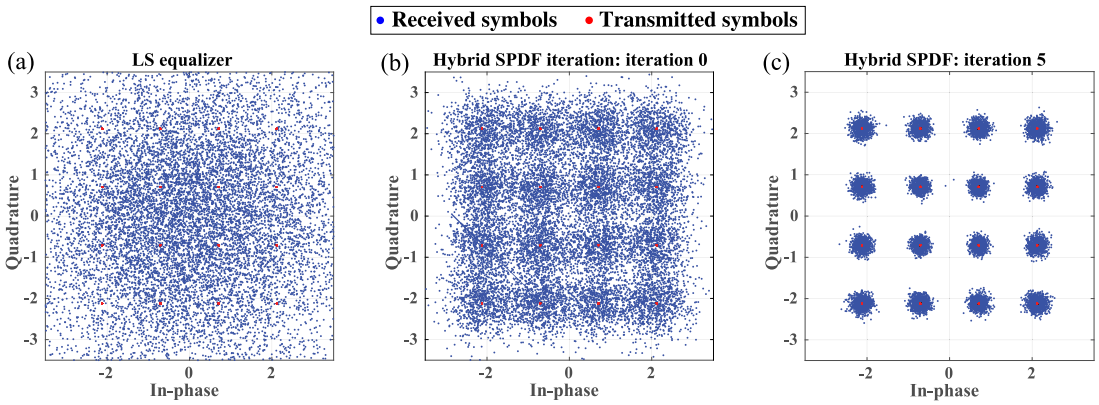

Fig. 7. IQ constellation points for different DSP receivers where the subcarrier spacing is 120 kHz and OPLL loop BW is 400 MHz: (a) standard OFDM receiver with least-squares (LS) equalizer corresponding to the blue blocks of Fig. 3; (b) hybrid SPDF method at iteration zero (after ULS estimation and compensation block of Fig. 3); (c) hybrid SPDF method after five iterations of the feedback loop.

Fig. 7 allows visualizing the BER reduction made by the proposed hybrid SPDF method. The received constellation points of Fig. 7(a) are obtained by using the standard OFDM receiver with leas-squares (LS) equalizer (blue blocks in Fig. 3 of the manuscript). In Figs. 7(b) and (c), the hybrid SPDF method is applied with zero and five iterations, respectively. The hybrid SPDF algorithm starts with IQ constellation points similar to those in Fig. 7(a). Then, with the ULS estimation and compensation block, the IQ constellations are as depicted in Fig. 7(b). Consequently, after five iterations in the decision feedback loop, the degradation induced by phase noise is almost completely compensated, as Fig. 7(c) shows. With this IQ constellation evolution through the hybrid SPDF method, the EVM and BER reductions of the proposed phase noise compensation method are clearly illustrated.

It is necessary to highlight that the channel equalizer in the decision feedback loop assumes a flat channel amplitude in order to achieve better performance. This assumptions is because the channel of the experimental setup does not include fades in the amplitude. Moreover, the cut-off frequency of the adaptive LPF in the decision feedback loop is set to be 2.5 MHz because the shape of this filter is adequately fitted respecting the OPLL phase noise of Fig. 2. Therefore, the attenuation of this adaptive filter decreases proportionally to the iteration number within the feedback loop from 30 to 5 dB. In this way, reduced restrictiveness of the adaptive filter is obtained and, thus, phase noise is estimated with more accuracy. Furthermore, the number of training pilots used in the ULS block is 35% of the total number of subcarrier pilots in the OFDM symbol [47]. Resulting from all these aspects, for each OPLL and OFDM configurations the number of required iterations of the decision feedback loop is three to accomplish the 5G requirements of 12.5% in 16-QAM, and better performance can be achieved using more iterations. Moreover, distributions of the constellations points are depicted in Fig. 6, for subcarrier spacing values of 15 kHz and 240 kHz and for different number of iterations of the decision feedback loop. This illustrates clearly the effective gain allowed by the hybrid SPDF method after 5 iterations. However, the achieved EVM tends toward a lower limit of the order of 5%–6%, which can be seen as the intrinsic limitation of the OPLL in terms of phase noise. These few percents represent the data that is, in average, not recovered because the added phase error is too high. This can be improved either by a more efficient algorithm or by a lower OPLL phase noise.

Finally, by comparing the graphs of Figs. 5 and 6, it can be determined that for 16-QAM the EVM converge point of the hybrid SPDF method is roughly equal to the achieved EVM using the RF-pilot assisted method (between 4 and 7.5% in every case). Then for this modulation format both methods satisfy the specifications according to 5G numerologies. Yet, concerning 64-QAM, the RF-pilot assisted method is still better due to the intrinsic phase noise of our OPLL being too high. An improved OPLL could be more suited to further evaluate the SPDF algorithm performance. That being said, the lower complexity at the IF stage of the proposed SPDF method makes it more advantageous in terms of resources from a system point of view. Therefore, this novel hybrid SPDF method is a promising path to be applied in OFDM ARoF systems with relatively high intrinsic phase noise, as for instance OPLLs, and using 5G numerologies.

5. Conclusions

In conclusion, we demonstrate in this study that the implemented OPLL is suitable for 16-QAM OFDM 5G data transmission in the n258 range if it is associated with a proper phase noise compensation method. This is a significant improvement compared to our previous experiment [8] where the phase noise was the limiting factor. The proposed OPLL setup allies high available optical power, high stability, standard commercial components and wide operating range as a counterpart of its medium phase noise. To exploit these advantages it is necessary to use a phase noise compensation method at the receiver side in order to mitigate its impact. Both methods used in this study, RF-pilot assisted and SPDF methods, are shown to be efficient enough to compensate the phase noise of the OPLL to meet the 5G requirements in the target frequency band. This has been shown experimentally for 16-QAM for both methods and for 64-QAM modulation format with RF-pilot assisted method. From a hardware point of view, a way to improve the OPLL would be either to use lower phase noise lasers, or to increase the BW of the loop, which is not easy given the fact we use DFB lasers. With a lower loop phase error variance then 64-QAM may eventually converge with the current hybrid SPDF algorithm but this has still to be investigated. As well the algorithm itself can still be improved, especially to make it compatible with real-time processing in order to ensure that enough iterations can be reached within a reasonable time compared to the rest of the processing. While ARoF has become one of the major solutions for the new mm-wave 5G fronthaul, the possibility to use relatively high phase noise but flexible implementation such as OPLLs is a very promising path toward future exploitation of mm-wave carriers for mobile communications.

Declaration of competing interest

The authors declare the following financial interests/personal relationships which may be considered as potential competing interests: This work was partially financed by the 5G STEP FWD and blueSPACE projects (GA nos. 722429 and 762055).

Data availability

Data will be made available on request.

Acknowledgments

This work was partially supported by the ITN 5G STEP-FWD and blueSPACE projects which have received funding from the European Union's Horizon2020 research and innovation programme under grant agreements No. 722429 and 762055.

References

[1] J.G. Andrews, et al., What will 5G be? IEEE J. Sel. Areas Commun. 32 (6) (2014) 1065–1082, http://dx.doi.org/10.1109/JSAC.2014.2328098.
[2] Cisco, Visual networking index, 2020, white paper URL https://www.cisco.com.
[3] T.S. Rappaport, et al., Millimeter wave mobile communications for 5G cellular: It will work!, IEEE Access 1 (2013) 335–349, http://dx.doi.org/10.1109/ACCESS.2013.2260813.
[4] M. Xiao, et al., Millimeter wave communications for future mobile networks, IEEE J. Sel. Areas Commun. 35 (9) (2017) 1909–1935, http://dx.doi.org/10.1109/JSAC.2017.2719924.
[5] A. Macho, M. Morant, R. Llorente, Next-generation optical fronthaul systems using multicore fiber media, J. Lightwave Technol. 34 (20) (2016) 4819–4827, http://dx.doi.org/10.1109/JLT.2016.2573038.
[6] C. Roeloffzen, et al., Enhanced coverage though optical beamforming in fiber wireless networks, in: 2017 19th International Conference on Transparent Optical Networks, ICTON, IEEE, Girona, Spain, 2017, pp. 1–4, http://dx.doi.org/10.1109/ICTON.2017.8025129.
[7] J. Liu, M. Sheng, L. Liu, J. Li, Network densification in 5G: From the short-range communications perspective, IEEE Commun. Mag. 55 (12) (2017) 96–102, http://dx.doi.org/10.1109/MCOM.2017.1700487.
[8] S. Rommel, et al., Towards a scaleable 5G fronthaul: Analog radio-over-fiber and space division multiplexing, J. Lightwave Technol. 38 (19) (2020) 5412–5422, http://dx.doi.org/10.1109/JLT.2020.3004416.
[9] D. Che, Analog vs digital radio-over-fiber: A spectral efficiency debate from the SNR perspective, J. Lightwave Technol. 39 (16) (2021) 5325–5335, http://dx.doi.org/10.1109/JLT.2021.3102220.
[10] A. Delmade, et al., Optical heterodyne analog radio-over-fiber link for millimeter-wave wireless systems, J. Lightwave Technol. 39 (2) (2021) 465–474, http://dx.doi.org/10.1109/JLT.2020.3032923.
[11] J. Brenes, et al., Network slicing architecture for SDM and analog-radio-over-fiber-based 5G fronthaul networks, J. Opt. Commun. Netw. 12 (4) (2020) B33–B43, http://dx.doi.org/10.1364/JOCN.381912.
[12] D. Konstantinou, et al., 5G RAN architecture based on analog radio-over-fiber fronthaul over UDWDM-PON and phased array fed reflector antennas, Opt. Commun. 454 (2020) 0030–4018, http://dx.doi.org/10.1016/j.optcom.2019.124464.
[13] J. Yu, Z. Jia, L. Yi, Y. Su, G.-K. Chang, T. Wang, Optical millimeter-wave generation or up-conversion using external modulators, IEEE Photonics Technol. Lett. 18 (1) (2006) 265–267, http://dx.doi.org/10.1109/LPT.2005.862006.
[14] J. Yao, Microwave photonics, J. Lightwave Technol. 27 (3) (2009) 314–335, http://dx.doi.org/10.1109/JLT.2008.2009551.
[15] P.J. Delfyett, et al., Optical frequency combs from semiconductor lasers and applications in ultrawideband signal processing and communications, J. Lightwave Technol. 24 (7) (2006) 2701–2719, http://dx.doi.org/10.1109/JLT.2006.875948.
[16] A. Delmade, et al., OFDM baud rate limitations in an optical heterodyne analog fronthaul link using unlocked fibre lasers, in: 2019 International Topical Meeting on Microwave Photonics, MWP, Ottawa, ON, Canada, 2019, pp. 1–4, http://dx.doi.org/10.1109/MWP.2019.8892190.
[17] E.P. Martin, et al., 25-Gb/s OFDM 60-GHz radio over fiber system based on a gain switched laser, J. Lightwave Technol. 33 (8) (2015) 1635–1643, http://dx.doi.org/10.1109/JLT.2015.2391994.
[18] K.-J. Boller, et al., Hybrid integrated semiconductor lasers with silicon nitride feedback circuits, Photonics 7 (1, 4) (2020) http://dx.doi.org/10.3390/photonics7010004.
[19] M.A. Tran, D. Huang, J.E. Bowers, Tutorial on narrow linewidth tunable semiconductor lasers using Si/III-V heterogeneous integration, APL Photonics 4 (11) (2019) 111101, http://dx.doi.org/10.1063/1.5124254.
[20] J.B. Armor, S.R. Robinson, Phase-lock control considerations for coherently combined lasers, Appl. Opt. 18 (18) (1979) 3165–3175, http://dx.doi.org/10.1364/AO.18.003165.
[21] U. Gliese, et al., A wideband heterodyne optical phase-locked loop for generation of 3-18 GHz microwave carriers, IEEE Photonics Technol. Lett. 4 (8) (1992) 936–938, http://dx.doi.org/10.1109/68.149915.
[22] L. Langley, et al., Packaged semiconductor laser optical phase-locked loop (OPLL) for photonic generation, processing and transmission of microwave signals, IEEE Trans. Microw. Theory Tech. 47 (7) (1999) 1257–1264, http://dx.doi.org/10.1109/22.775465.
[23] S. Ristic, et al., An optical phase-locked loop photonic integrated circuit, J. Lightwave Technol. 28 (4) (2009) 526–538, http://dx.doi.org/10.1109/JLT.2009.2030341.
[24] K. Balakier, L. Ponnampalam, M.J. Fice, C.C. Renaud, A.J. Seeds, Integrated semiconductor laser optical phase lock loops, IEEE J. Sel. Top. Quantum Electron. 24 (1) (2017) 1–12, http://dx.doi.org/10.1109/JSTQE.2017.2711581.
[25] S. Arafin, A. Simsek, M. Lu, M.J. Rodwell, L.A. Coldren, Heterodyne locking of a fully integrated optical phase-locked loop with on-chip modulators, Opt. Lett. 42 (19) (2017) 3745–3748, http://dx.doi.org/10.1364/OL.42.003745.
[26] A.A. Zaidi, et al., Waveform and numerology to support 5G services and requirements, IEEE Commun. Mag. 54 (11) (2016) 90–98, http://dx.doi.org/10.1109/MCOM.2016.1600336CM.
[27] J.P. Santacruz, S. Rommel, U. Johannsen, A. Jurado-Navas, I.T. Monroy, Candidate waveforms for ARoF in beyond 5G, Appl. Sci. 10, 3891 (11) (2020) http://dx.doi.org/10.3390/app10113891.
[28] D. Dass, S. O'Duill, A. Delmade, C. Browning, Analysis of phase noise in a hybrid photonic/millimetre-wave system for single and multi-carrier radio applications, Appl. Sci. 10, 5800 (17) (2020) http://dx.doi.org/10.3390/app10175800.
[29] F.M. Gardner, Phaselock Techniques, John Wiley & Sons, 2005.
[30] R. Muñoz, et al., Experimental demonstration of dynamic optical beamforming for beyond 5G spatially multiplexed fronthaul networks, IEEE J. Sel. Top. Quantum Electron. 27 (6) (2021) 1–16, http://dx.doi.org/10.1109/JSTQE.2021.3079726.
[31] F. Ashtiani, P. Sanjari, M.H. Idjadi, F. Aflatouni, High-resolution optical frequency synthesis using an integrated electro-optical phase-locked loop, IEEE Trans. Microw. Theory Tech. 66 (12) (2018) 5922–5932, http://dx.doi.org/10.1109/TMTT.2018.2878567.
[32] W. Liang, A. Yariv, A. Kewitsch, G. Rakuljic, Coherent combining of the output of two semiconductor lasers using optical phase-lock loops, Opt. Lett. 32 (4) (2007) 370–372, http://dx.doi.org/10.1364/OL.32.000370.
[33] L.A. Coldren, S.W. Corzine, M.L. Mashanovitch, Diode Lasers and Photonic Integrated Circuits, Vol. 218, John Wiley & Sons, 2012.
[34] L. Ponnampalam, et al., Monolithically integrated photonic heterodyne system, J. Lightwave Technol. 29 (15) (2011) 2229–2234, http://dx.doi.org/10.1109/JLT.2011.2158186.
[35] M. Lu, et al., An integrated 40 Gbit/s optical costas receiver, J. Lightwave Technol. 31 (13) (2013) 2244–2253, http://dx.doi.org/10.1109/JLT.2013.2265075.
[36] A. Bordonalli, C. Walton, A.J. Seeds, High-performance phase locking of wide linewidth semiconductor lasers by combined use of optical injection locking and optical phase-lock loop, J. Lightwave Technol. 17 (2) (1999) 328, http://dx.doi.org/10.1109/50.744252.
[37] L.S. Cutler, C.L. Searle, Some aspects of the theory and measurement of frequency fluctuations in frequency standards, Proc. IEEE 54 (2) (1966) 136–154, http://dx.doi.org/10.1109/PROC.1966.4627.
[38] 3GPP, FG IMT-2020: User equipment (UE) radio transmission and reception; part 2: Range 2 standalone. 3GPP TS 38.101-2, version 17.4.0, release 17, 2021.
[39] K. Zeb, Z. Lu, J. Liu, Y. Mao, G. Liu, P.J. Poole, C. Song, M. Rahim, G. Pakulski, P. Barrios, X. Zhang, A quantum dash mode-locked laser-based photonic aided broadband multi-Gb/s wireless signal delivery system at 5G NR, in: Broadband Access Communication Technologies XV, Vol. 11711, 2021, pp. 65–70, http://dx.doi.org/10.1117/12.2583066.
[40] G. Jacobsen, T. Xu, S. Popov, J. Li, A.T. Friberg, Y. Zhang, Receiver implemented RF pilot tone phase noise mitigation in coherent optical nPSK and nQAM systems, Opt. Express 19 (15) (2011) 14487–14494, http://dx.doi.org/10.1364/OE.19.014487.
[41] T. Shao, E. Martin, P.M. Anandarajah, C. Browning, V. Vujicic, R. Llorente, L.P. Barry, Chromatic dispersion-induced optical phase decorrelation in a 60 GHz OFDM-RoF system, IEEE Photonics Technol. Lett. 26 (20) (2014) 2016–2019, http://dx.doi.org/10.1109/LPT.2014.2344314.
[42] C.-C. Wei, C.-T. Lin, H.-T. Huang, W.-L. Liang, S. Chi, Estimation and suppression of dispersion-induced phase noise in W-band direct-detection OFDM radio-over-fiber systems, J. Lightwave Technol. 32 (20) (2014) 3874–3884, http://dx.doi.org/10.1109/JLT.2014.2322601.
[43] A. Delmade, C. Browning, T. Verolet, J. Poette, A. Farhang, H.H. Elwan, R.D. Koilpillai, G. Aubin, F. Lelarge, A. Ramdane, D. Venkitesh, L.P. Barry, Optical heterodyne analog radio-over-fiber link for millimeter-wave wireless systems, J. Lightwave Technol. 39 (2) (2021) 465–474, http://dx.doi.org/10.1109/JLT.2020.3032923.
[44] J. Perez Santacruz, S. Rommel, U. Johannsen, A. Jurado-Navas, I. Tafur Monroy, Analysis and compensation of phase noise in mm-wave OFDM ARoF systems for beyond 5G, J. Lightwave Technol. 39 (6) (2021) 1602–1610, http://dx.doi.org/10.1109/JLT.2020.3041041.
[45] W.-R. Peng, T. Tsuritani, I. Morita, Simple carrier recovery approach for RF-pilot-assisted PDM-CO-OFDM systems, J. Lightwave Technol. 31 (15) (2013) 2555–2564, http://dx.doi.org/10.1109/JLT.2013.2270551.
[46] P. Mathecken, T. Riihonen, S. Werner, R. Wichman, Constrained phase noise estimation in OFDM using scattered pilots without decision feedback, IEEE Trans. Signal Process. 65 (9) (2017) 2348–2362, http://dx.doi.org/10.1109/TSP.2017.2655481.
[47] R.A. Casas, S.L. Biracree, A.E. Youtz, Time domain phase noise correction for OFDM signals, IEEE Trans. Broadcast. 48 (3) (2002) 230–236, http://dx.doi.org/10.1109/TBC.2002.803711.